

Modelization of the EOS

C. Fuchs¹ and H.H. Wolter²

¹ Institut für Theoretische Physik der Universität Tübingen, D-72076 Tübingen, Germany

² Sektion Physik der Universität München, D-85748 Garching, Germany

Received: date / Revised version: date

Abstract. This article summarizes theoretical predictions for the density and isospin dependence of the nuclear mean field and the corresponding nuclear equation of state. We compare predictions from microscopic and phenomenological approaches. An application to heavy ion reactions requires to incorporate these forces into the framework of dynamical transport models. Constraints on the nuclear equation of state derived from finite nuclei and from heavy ion reactions are discussed.

PACS. 21.65.+f – 21.60.-n – 21.30.-x – 24.10.Cn – 25.75.-q – 25.60.Gc – 25.70.Mn

1 Introduction

Heavy ion reactions provide the only possibility to reach nuclear matter densities beyond saturation density $\rho_0 \simeq 0.16 \text{ fm}^{-3}$. Transport calculations indicate that in the low and intermediate energy range $E_{\text{lab}} \sim 0.1 \div 1 \text{ AGeV}$ nuclear densities between $2 \div 3\rho_0$ are accessible while the highest baryon densities ($\sim 8\rho_0$) will probably be reached in the energy range of the future GSI facility FAIR between $20 \div 30 \text{ AGeV}$. At even higher incident energies transparency sets in and the matter becomes less baryon rich due to the dominance of meson production. The isospin dependence of the nuclear forces which is at present only little constrained by data will be explored by the forthcoming radioactive beam facilities at FAIR/GSI [1], SPIRAL2/GANIL and RIA [2]. Since the knowledge of the nuclear equation-of-state (EOS) at supra-normal densities and extreme isospin is essential for our understanding of the nuclear forces as well as for astrophysical purposes, the determination of the EOS was already one of the primary goals when first relativistic heavy ion beams started to operate in the beginning of the 80ties [3]. In the following we will briefly discuss the knowledge on the nuclear EOS from a theoretical point of view, then turn to the realization within transport models, and finally give a short review on possible observables from heavy ion reactions to constrain the EOS.

2 Models for the nuclear EOS

Models which make predictions on the nuclear EOS can roughly be divided into three classes:

1. **Phenomenological density functionals:** These are models based on effective density dependent interactions such as Gogny [4,5] or Skyrme forces [6,7] or relativistic mean field (RMF) models [8]. The number of

parameters which are fine tuned to the nuclear chart is usually larger than six and less than 15. This type of models allows the most precise description of finite nuclei properties.

2. **Effective field theory approaches:** Models where the effective interactions is determined within the spirit of effective field theory (EFT) became recently more and more popular. Such approaches lead to a more systematic expansion of the EOS in powers of density, respectively the Fermi momentum k_F . They can be based on density functional theory [9,10] or e.g. on chiral perturbation theory [11,12,13]. The advantage of EFT is the small number of free parameters and a correspondingly higher predictive power. However, when high precision fits to finite nuclei are intended this is presently only possible by the price of fine tuning through additional parameters. Then EFT functionals are based on approximately the same number of model parameters as phenomenological density functionals.
3. **Ab initio approaches:** Based on high precision free space nucleon-nucleon interactions, the nuclear many-body problem is treated microscopically. Predictions for the nuclear EOS are parameter free. Examples are variational calculations [14,15], Brueckner-Hartree-Fock (BHF) [16,17,18,19] or relativistic Dirac-Brueckner-Hartree-Fock (DBHF) [20,21,22,23,24,25,26] calculations and Greens functions Monte-Carlo approaches [27,28,29].

Phenomenological models as well as EFT contain parameters which have to be fixed by nuclear properties around or below saturation density which makes the extrapolation to supra-normal densities somewhat questionable. However, in the EFT case such an extrapolation is safer due to a systematic density expansion. One has nevertheless, to keep in mind that EFT approaches are based on low density expansions. Many-body calculations, on the other hand, have to rely on the summation of relevant diagram classes

and are still too involved for systematic applications to finite nuclei.

2.1 Mean field theory

Among non-relativistic density functionals are Skyrme functionals most frequently used. The Skyrme interaction contains an attractive local two-body part and a repulsive density dependent two-body interaction which can be motivated by local three-body forces. We will not consider surface terms which involve gradients as well as spin-orbit contributions since they vanish in infinite nuclear matter. For a detailed discussion of Skyrme functionals and their relation to relativistic mean field (RMF) theory see e.g. [7]. The EOS of symmetric nuclear matter, i.e. the binding energy per particle has the simple form

$$E/A = \frac{3k_F^2}{10M} + \frac{\alpha}{2}\rho + \frac{\beta}{1+\gamma}\rho^\gamma , \quad (1)$$

where the first term in (1) represents the kinetic energy of a non-relativistic Fermi gas and the remaining part the potential energy. To examine the structure of relativistic mean field models it is instructive to consider the simplest version of a relativistic model, i.e. the $\sigma\omega$ model of Quantum Hadron Dynamics (QHD-I) [30]. In QHD-I the nucleon-nucleon interaction is mediated by the exchange of two effective boson fields which are attributed to a scalar σ and a vector ω meson. The energy density in infinite cold and isospin saturated nuclear matter is in mean field approximation given by

$$\epsilon = \frac{3}{4}E_F\rho + \frac{1}{4}m_D^*\rho_S + \frac{1}{2}\{\Gamma_V\rho^2 + \Gamma_S\rho_S^2\} , \quad (2)$$

where the Fermi energy is given by $E_F = \sqrt{k_F^2 + m_D^{*2}}$. We will denote m_D^* explicitly as Dirac mass in the following in order to distinguish it from its non-relativistic counterpart. The effective mass absorbs the scalar part of the mean field $m_D^* = M - \Gamma_S\rho_S$. In the limit $m_D^* \rightarrow M$ the first two terms in (2) provide the energy (kinetic plus rest mass) of a non-interacting relativistic Fermi gas.

A genuine feature of all relativistic models is the fact that one has to distinguish between the vector density $\rho = 2k_F^3/3\pi^2$ and a scalar density ρ_S . The vector density is the time-like component of a 4-vector current j_μ which spatial components vanish in the nuclear matter rest frame, while ρ_S is a Lorentz scalar. The scalar density shows a saturation behavior with increasing vector density which is essential for the relativistic saturation mechanism. This becomes clear when binding energy $E/A = \epsilon/\rho - M$ is expanded in powers of the Fermi momentum k_F

$$E/A = \left[\frac{3k_F^2}{10M} - \frac{3k_F^4}{56M^3} + \dots \right] + \frac{1}{2}\left[\Gamma_V - \Gamma_S\right]\rho \quad (3)$$

$$+ \Gamma_S \frac{\rho}{M} \left[\frac{3k_F^2}{10M} - \frac{36k_F^2}{175M^3} + \dots \right] + \mathcal{O}((\Gamma_S\rho/M)^2)$$

The first term in (3) contains the kinetic energy of a non-relativistic Fermi gas followed by relativistic corrections

and the remaining terms are the contributions from the mean field. In QHD-I the scalar and vector field strengths are given by the coupling constants for the corresponding mesons $\Gamma_S = g_\sigma^2/m_\sigma^2$ and $\Gamma_V = g_\omega^2/m_\omega^2$ divided by the meson masses. The two parameters $\Gamma_{S,V}$ are now fitted to the saturation point of nuclear matter $E/A \simeq -16$ MeV, $\rho_0 \simeq 0.16 \text{ fm}^{-3}$ which follows from the volume part of the Weizäcker mass formula. The saturation mechanism requires that both coupling constants are large. This leads automatically to the cancellation of two large fields, namely an attractive scalar field $\Sigma_S = -\Gamma_S\rho_S$ and a repulsive vector field $\Sigma_V = \Gamma_V\rho$. As is a typical feature of relativistic dynamics the single particle potential $U = m_D^*/E^* \Sigma_S - \Sigma_V$ ($E^* = \sqrt{\mathbf{k}^2 + m_D^{*2}}$), which is of the order of -50 MeV, results from the cancellation of scalar and vector fields, each of the order of several hundred MeV.

However, with only two parameters QHD-I provides a relatively poor description of the saturation point with a too large saturation density and a very stiff EOS (K=540 MeV). To improve on this higher order corrections in density have to be taken into account. This can be done in several ways: In the spirit of the original Walecka model non-linear meson self-interaction terms have been introduced into the QHD Lagrangian [8,31]. An alternative are relativistic point coupling models where the explicit meson exchange picture is abandoned. A Lagrangian of nucleon and boson fields with point couplings can be constructed in the spirit of EFT and expanded in powers of density [9,10]. Finite range effects from meson propagators are replaced by density gradients [9,10]. A third possibility is density dependent hadron field theory DDRH [32,33]. In DDRH the scalar and vector coupling constants are replaced by density dependent vertex functions $\Gamma_{S,V}(k_F)$. The density dependence of these renormalized vertices can either be taken from Brueckner calculations thus parameterizing many-body correlations [32,33] or be determined phenomenologically [34,35]. In all cases additional parameters are introduced which allow a description of finite nuclei with a precision comparable to the best fits from Skyrme functionals. Phenomenological density functionals provide high quality fits to the known areas of the nuclear chart. Binding energies and rms-radii are reproduced with an average relative error of about $\sim 1-5\%$. However, when the various models are extrapolated to the unknown regions of extreme isospin or to super-heavies predictions start to deviate substantially. This demonstrates the limited predictive power of these functionals.

2.2 Effective field theory

When concepts of effective field theory are applied to nuclear physics problem one has to rely on a separation of scales. EFT is based on a perturbative expansion of the nucleon-nucleon (NN) interaction or the nuclear mean field within power counting schemes. The short-range part of the NN interaction requires a non-perturbative treatment, e.g. within the Brueckner ladder summation. The

philosophy behind EFT is to separate short-range correlations from the long and intermediate range part of the NN-interaction. This assumption is motivated by the fact that the scale of the short-range correlations, i.e. the hard core, is set by the ρ and ω vector mesons masses which lie well above the Fermi momentum and the pion mass which sets the scale of the long range forces. The density

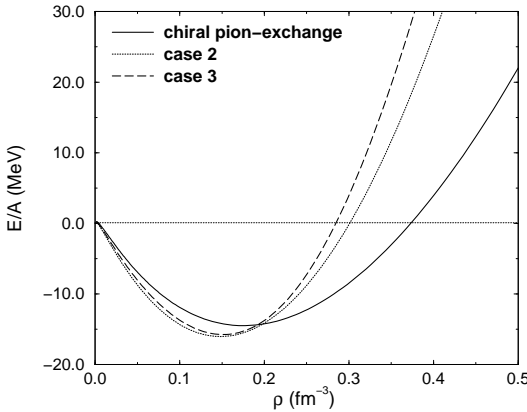


Fig. 1. EOS for symmetric nuclear matter obtained from chiral one- and two-pion exchange (case 1, solid curve), by adding background fields from QCD sum rules, and finally after fine tuning to finite nuclei properties (case 3, dashed curve). Figure is taken from [12].

functional theory (DFT) formulation of the relativistic nuclear many-body problem [9,10] is thereby analogous to the Kohn-Sham approach in DFT. An energy functional of scalar and vector densities is constructed which by minimization gives rise to variational equations that determine the ground-state densities. Doing so, one tries to approximate the *exact* functional using an expansion in classical meson fields and their derivatives, based on the observation that the ratios of these quantities to the nucleon mass are small, at least up to moderate density. The exact energy functional which one tries to derive explicitly when using many-body techniques such as Brueckner or variational approaches contains exchange-correlation and all other many-body and relativistic effects. The DFT interpretation implies that the model parameters fitted to nuclei implicitly contain effects of both short-distance physics and many-body corrections.

Recently also concepts of chiral perturbation theory (ChPT) have been applied to the nuclear many-body problem [12,13]. Doing so, the long and intermediate-range interactions are treated explicitly within chiral pion-nucleon dynamics. This allows an expansion of the energy density functional in powers of m_π/M or in k_F/M . Like in DFT, short-range correlation are not resolved explicitly but handled by counter-terms (dimensional regularization) [11] or through a cut-off regularization [13]. Fig. 1 shows the corresponding EOS obtained from chiral one- and two-pion exchange between nucleons. In order to account for the most striking feature of relativistic dynamics, expressed by the existence of the large scalar and vector fields, in

Refs. [12,13] iso-scalar condensate background nucleon self-energies derived from QCD sum rules have been added to the chiral fluctuations. To lowest order in density the QCD condensates give rise to a scalar self-energy $\Sigma_S = -\sigma_N M/(m_\pi^2 f_\pi^2) \varrho_S$ and a vector self-energy $\Sigma_V = 4(m_u + m_d) M/(m_\pi^2 f_\pi^2) \varrho$. It is remarkable that the total self-energies, i.e. condensates plus chiral fluctuations, are very close to those obtained from DBHF calculations [12,23]. The resulting EOS is also shown in Fig. 1 in addition with that obtained after fine tuning to finite nuclei. Although the original EOS (case 1) is rather soft the inclusion of the condensates and the adjustment to finite nuclei results in an EOS with is finally stiff.

2.3 Ab initio calculations

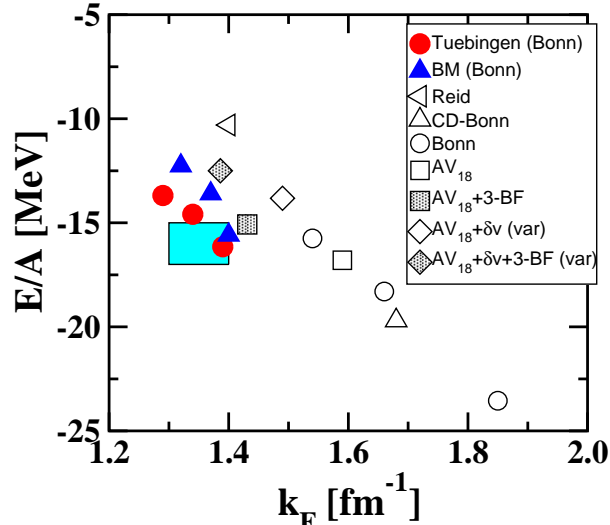


Fig. 2. Nuclear matter saturation points from relativistic (full symbols) and non-relativistic (open symbols) Brueckner-Hartree-Fock calculations based on different nucleon-nucleon forces. The diamonds show results from variational calculations. Shaded symbols denote calculations which include 3-body forces. The shaded area is the empirical region of saturation.

In *ab initio* calculations based on many-body techniques one derives the energy functional from first principles, i.e. treating short-range and many-body correlations explicitly. A typical example for a successful many-body approach is Brueckner theory [16]. In the relativistic Brueckner approach the nucleon inside the medium is dressed by the self-energy Σ . The in-medium T-matrix which is obtained from the relativistic Bethe-Salpeter (BS) equation plays the role of an effective two-body interaction which contains all short-range and many-body correlations of the ladder approximation. Solving the BS-equation the Pauli principle is respected and intermediate scattering states are projected out of the Fermi sea. The summation of the T-matrix over the occupied states inside the Fermi sea yields finally the self-energy in Hartree-Fock

approximation. This coupled set of equations states a self-consistency problem which has to be solved by iteration.

In contrast to relativistic DBHF calculations which came up in the late 80ties non-relativistic BHF theory has already almost half a century's history. The first numerical calculations for nuclear matter were carried out by Brueckner and Gammel in 1958 [16]. Despite strong efforts invested in the development of improved solution techniques for the Bethe-Goldstone (BG) equation, the non-relativistic counterpart of the BS equation, it turned out that, although such calculations were able to describe the nuclear saturation mechanism qualitatively, they failed quantitatively. Systematic studies for a large number of NN interactions were always allocated on a so-called *Coester line* in the $E/A - \rho$ plane which does not meet the empirical region of saturation. In particular modern one-boson-exchange (OBE) potentials lead to strong over-binding and too large saturation densities where relativistic calculations do a much better job.

Fig. 2 compares the saturation points of nuclear matter obtained by relativistic Dirac-Brueckner-Hartree-Fock (DBHF) calculations using the Bonn potentials [36] as bare NN interactions to non-relativistic Brueckner-Hartree-Fock calculations for various NN interactions. The DBHF results are taken from Ref. [21] (BM) and more recent calculations based on improved techniques are from [23] (Tübingen). Several reasons have been discussed in the

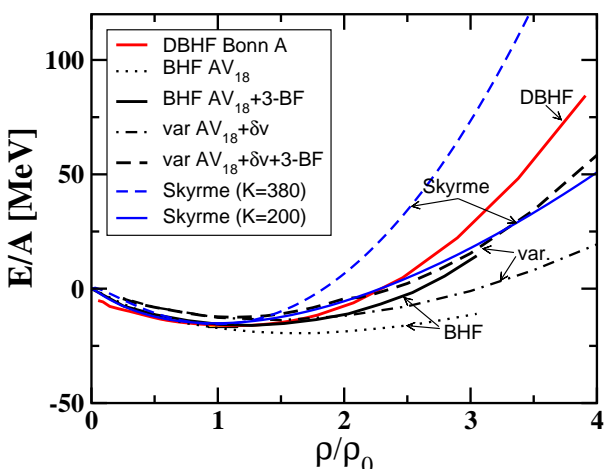


Fig. 3. Predictions for the EOS of symmetric nuclear matter from microscopic ab initio calculations, i.e. relativistic DBHF [23], non-relativistic BHF [18] and variational [15] calculations. For comparison also soft and hard Skyrme forces are shown.

literature in order to explain the success of the relativistic treatment. The saturation mechanisms in relativistic and non-relativistic theories are quite different. In relativistic MFT the vector field grows linear with density while the scalar field saturates at large densities. The magnitude and the density dependence of the scalar and vector DBHF self-energy is similar to MFT, i.e. the single particle potential is the result of the cancellation of two large scalar and vector fields, each several hundred MeV

in magnitude (see e.g. the effective mass in Fig. 7). In BHF, on the other hand, the saturation mechanism takes place exclusively on the scale of the binding energy, i.e. a few ten MeV. It cannot be understood by the absence of a tensor force. In particular the second order $1-\pi$ exchange potential (OPEP) is large and attractive at high densities and its interplay with Pauli-blocking leads finally to saturation. Relativistically the tensor force is quenched by a factor $(m_D^*/M)^2$ and less important for the saturation mechanism [37].

Three-body forces (3-BFs) have extensively been studied within non-relativistic BHF [18] and variational calculations [15]. The contributions from 3-BFs are in total repulsive which makes the EOS harder and non-relativistic calculations come close to their relativistic counterparts. The same effect is observed in variational calculations [15] shown in Fig. 3. The variational results shown contain boost corrections (δv) which account for relativistic kinematics and lead to additional repulsion [15]. Both, BHF [18] and the variational calculations from [15] are based on the latest AV₁₈ version of the Argonne potential. In both cases phenomenological 3-body-forces are used, the Tucson-Melbourne 3-BF in [18] and the Urbana IX 3-BF¹ in [15]. It is often argued that in non-relativistic treatments 3-BFs play in some sense an equivalent role as the dressing of the two-body interaction by in-medium spinors in Dirac phenomenology. Both mechanisms lead indeed to an effective density dependent two-body interaction V which is, however, of different origin. One class of 3-BFs involves virtual excitations of nucleon-antinucleon pairs. Such Z-graphs are in net repulsive and can be considered as a renormalization of the meson vertices and propagators. A second class of 3-BFs is related to the inclusion of explicit resonance degrees of freedom. The most important resonance is the $\Delta(1232)$ isobar which provides at low and intermediate energies large part of the intermediate range attraction. Intermediate Δ states appear in elastic NN scattering only in combination with at least two-isovector-meson exchange ($\pi\pi, \pi\rho, \dots$). Such box diagrams can satisfactorily be absorbed into an effective σ -exchange [36]. The maintenance of explicit Δ DoFs gives rise to additional saturation, shifting the saturation point away from the empirical region [20]. However, as pointed out e.g. in [27] the inclusion of non-nucleonic DoFs has to be performed with caution: Freezing out resonance DoFs generates automatically a class of three-body forces which contains nucleon-resonance excitations. There exist strong cancellation effects between the repulsion due to box diagrams and contributions from 3-BFs. Non-nucleonic DoFs and many-body forces should therefore be treated on the same footing. Such a treatment may be possible with the next generation of nucleon-nucleon forces based on chiral perturbation theory [38,39] which allows a systematic generation of three-body forces. Next-to-leading order all 3-BFs cancel while non-vanishing contributions appear at NNLO.

¹ Using boost corrections the repulsive contributions of the UIX interaction are reduced by about 40% compared to the original ones in [15]

Fig. 3 compares the equations of state from the different approaches: DBHF from Ref. [23] based the Bonn A interaction² [36], BHF [18] and variational calculations [15]. The latter ones are based on the Argonne AV₁₈ potential and include 3-body forces. All the approaches use modern high precision NN interactions and represent state of the art calculations. Two phenomenological Skyrme functionals which correspond to the limiting cases of a soft ($K=200$ MeV) and a hard ($K=380$ MeV) EOS are shown as well. In contrast to the Skyrme interaction (1) where the high density behavior is fixed by the compression modulus, in microscopic approaches the compression modulus is only loosely connected to the curvature at saturation density. DBHF Bonn A has e.g. a compressibility of $K=230$ MeV. Below $3\rho_0$ both are not too far from the soft Skyrme EOS. The same is true for BHF including 3-body forces.

When many-body calculations are performed, one has to keep in mind that elastic NN scattering data constrain the interaction only up to about 400 MeV, which corresponds to the pion threshold. NN potentials differ essentially in the treatment of the short-range part. A model independent representation of the NN interaction can be obtained in EFT approaches where the unresolved short distance physics is replaced by simple contact terms. In the framework of chiral EFT the NN interaction has been computed up to N^3LO [39,40]. An alternative approach which leads to similar results is based on renormalization group (RG) methods [41]. In the $V_{\text{low } k}$ approach a low-momentum potential is derived from a given realistic NN potential by integrating out the high-momentum modes using RG methods. At a cutoff $\Lambda \sim 2 \text{ fm}^{-1}$ all the different NN potential models were found to collapse to a model-independent effective interaction $V_{\text{low } k}$. When applied to the nuclear many-body problem low momentum interactions do not require a full resummation of the Brueckner ladder diagrams but can already be treated within second-order perturbation theory [42]. However, without repulsive three-body-forces isospin saturated nuclear matter was found to collapse. Including 3-BFs first promising results have been obtained with $V_{\text{low } k}$ [42], however, nuclear saturation is not yet described quantitatively. Moreover, one has to keep in mind that - due to the high momentum cut-offs - EFT is essentially suitable at moderate densities.

3 EOS in symmetric and asymmetric nuclear matter

Fig. 4 compares now the predictions for nuclear and neutron matter from microscopic many-body calculations – DBHF [26] and the ‘best’ variational calculation with 3-BFs and boost corrections [15] – to phenomenological approaches and to EFT. As typical examples for relativistic functionals we take NL3 [43] as one of the best RMF fits to the nuclear chart and a phenomenological density dependent RMF functional DD-TW from [34]. ChPT+corr. is

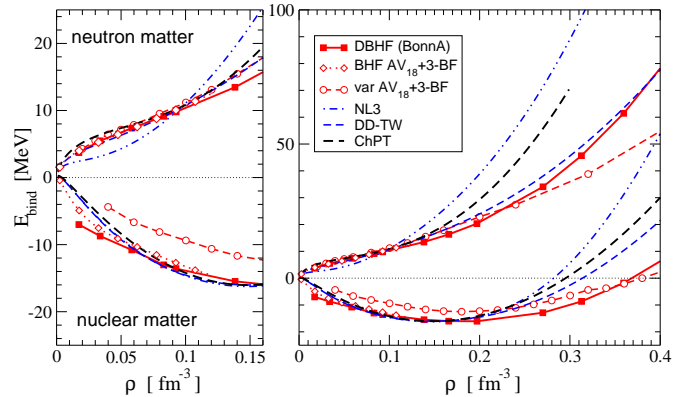


Fig. 4. EOS in nuclear matter and neutron matter. BHF/DBHF and variational calculations are compared to phenomenological density functionals NL3 and DD-TW and ChPT+corr.. The left panel zooms the low density range.

based on chiral pion-nucleon dynamics including condensate fields and fine tuning to finite nuclei (case 3 in Fig. 1). As expected the phenomenological functionals agree well at and below saturation density where they are constrained by finite nuclei, but start to deviate substantially at supra-normal densities. In neutron matter the situation is even worse since the isospin dependence of the phenomenological functionals is less constrained. The predictive power of such density functionals at supra-normal densities is restricted. *Ab initio* calculations predict throughout a soft EOS in the density range relevant for heavy ion reactions at intermediate and low energies, i.e. up to about three times ρ_0 . There seems to be no way to obtain an EOS as stiff as the hard Skyrme force shown in Fig. 3 or NL3. Since the nn scattering length is large, neutron matter at subnuclear densities is less model dependent. The microscopic calculations (BHF/DBHF, variational) agree well and results are consistent with ‘exact’ Quantum-Monte-Carlo calculations [29].

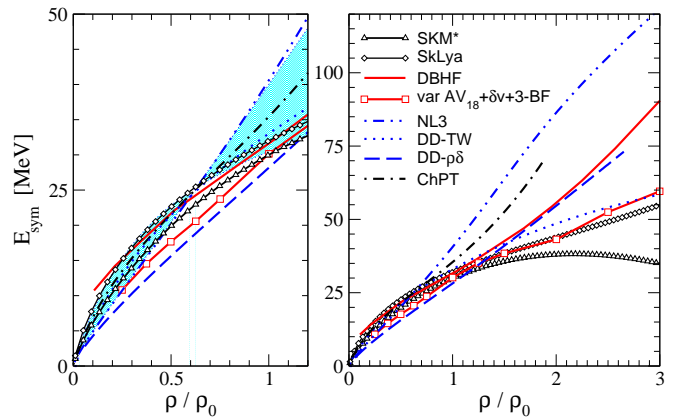


Fig. 5. Symmetry energy as a function of density as predicted by different models. The left panel shows the low density region while the right panel displays the high density range.

² The high density behavior of the EOS obtained with different interaction, e.g. Bonn B or C is very similar. [23]

In isospin asymmetric matter the binding energy is a functional of the proton and neutron densities, characterized by the asymmetry parameter $\beta = Y_n - Y_p$ which is the difference of the neutron and proton fraction $Y_i = \rho_i/\rho$, $i = n, p$. The isospin dependence of the energy functional can be expanded in terms of β which leads to a parabolic dependence on the asymmetry parameter

$$E(\rho, \beta) = E(\rho) + E_{\text{sym}}(\rho)\beta^2 + \mathcal{O}(\beta^4) + \dots$$

$$E_{\text{sym}}(\rho) = \frac{1}{2} \frac{\partial^2 E(\rho, \beta)}{\partial \beta^2} \Big|_{\beta=0} = a_4 + \frac{p_0}{\rho_0^2}(\rho - \rho_0) + \dots \quad (4)$$

Fig. 5 compares the symmetry energy predicted from the DBHF and variational calculations to that of the empirical density functionals already shown in Fig. 4. In addition the relativistic DD- $\rho\delta$ RMF functional [44] is included. Two Skyrme functionals, SkM* and the more recent Skyrme-Lyon force SkLya represent non-relativistic models. The left panel zooms the low density region while the right panel shows the high density behavior of E_{sym} . Remarkable is that most empirical models coincide around $\rho \simeq 0.6\rho_0$ where $E_{\text{sym}} \simeq 24$ MeV. This demonstrates that constraints from finite nuclei are active for an average density slightly above half saturation density. However, the extrapolations to supra-normal densities diverge dramatically. This is crucial since the high density behavior of E_{sym} is essential for the structure and the stability of neutron stars (see also the discussion in Sec. V.5). The microscopic models show a density dependence which can still be considered as *asy-stiff*. DBHF [26] is thereby stiffer than the variational results of [15]. The density dependence is generally more complex than in RMF theory, in particular at high densities where E_{sym} shows a non-linear and more pronounced increase. Fig. 5 clearly demonstrates the necessity to constrain the symmetry energy at supra-normal densities with the help of heavy ion reactions. The

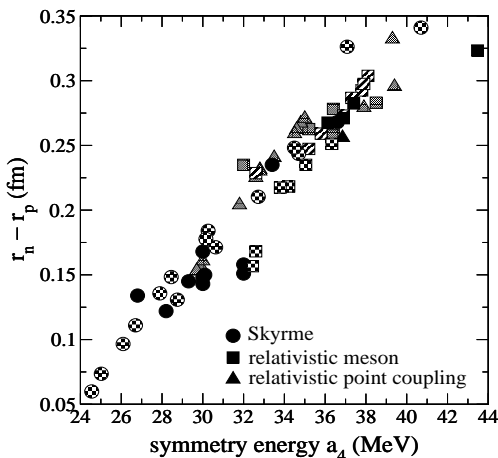


Fig. 6. Skin thickness in ^{208}Pb versus the linear symmetry energy parameter a_4 for various models. Figure is taken from [10].

hatched area in Fig. 5 displays the range of E_{sym} which has been obtained by constructing a density dependent RMF

functional varying thereby the linear asymmetry parameter a_4 from 30 to 38 MeV [35]. In [35] it was concluded that charge radii, in particular the skin thickness $r_n - r_p$ in heavy nuclei constrains the allowed range of a_4 to $32 \div 36$ MeV for relativistic functionals.

Fig. 6 displays the correlation between the skin thickness in ^{208}Pb and a_4 obtained within various models. The skin thickness depends, however, not only on the symmetry energy but there exists a close correlation between a_4 and the compression modulus K [35]. This correlation is of importance when these quantities are extracted from finite nuclei (see discussion by Shlomo et al. in Sec. I.4).

3.1 Effective nucleon masses

The introduction of an effective mass is a common concept to characterize the quasi-particle properties of a particle inside a strongly interacting medium. In nuclear physics exist different definitions of the effective nucleon mass which are often compared and sometimes even mixed up: the non-relativistic effective mass m_{NR}^* and the relativistic Dirac mass m_D^* . These two definitions are based on different physical concepts. The nonrelativistic mass parameterizes the momentum dependence of the single-particle potential. The relativistic Dirac mass is defined through the scalar part of the nucleon self-energy in the Dirac field equation which is absorbed into the effective mass $m_D^* = M + \Sigma_S(k, k_F)$. The Dirac mass is a smooth function of the momentum. In contrast, the nonrelativistic effective mass - as a model independent result - shows a narrow enhancement near the Fermi surface due to an enhanced level density [45]. For a recent review on this subject and experimental constraints on m_{NR}^* see [46].

While the Dirac mass is a genuine relativistic quantity the effective mass m_{NR}^* is determined by the single-particle energy

$$m_{NR}^* = k[dE/dk]^{-1} = \left[\frac{1}{M} + \frac{1}{k} \frac{d}{dk} U \right]^{-1}. \quad (5)$$

m_{NR}^* is a measure of the non-locality of the single-particle

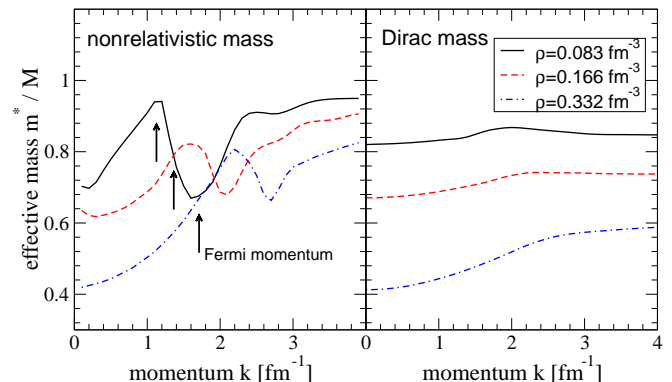


Fig. 7. The effective mass in isospin symmetric nuclear matter as a function of the momentum k at different densities determined from relativistic Brueckner calculations.

potential U (real part) which can be due to non-localities in space, resulting in a momentum dependence, or in time, resulting in an energy dependence. In order to clearly separate both effects, one has to distinguish further between the so-called k -mass and the E -mass [17]. The spatial non-localities of U are mainly generated by exchange Fock terms and the resulting k -mass is a smooth function of the momentum. Non-localities in time are generated by Brueckner ladder correlations due to the scattering to intermediate states which are off-shell. These are mainly short-range correlations which generate a strong momentum dependence with a characteristic enhancement of the E -mass slightly above the Fermi surface [45,17,47]. The effective mass defined by Eq. (5) contains both, non-localities in space and time and is given by the product of k -mass and E -mass [17]. In Fig. 7 the nonrelativistic effective mass and the Dirac mass, both determined from DBHF calculations [48], are shown as a function of momentum k at different Fermi momenta of $k_F = 1.07, 1.35, 1.7 \text{ fm}^{-1}$. m_{NR}^* shows the typical peak structure as a function of momentum around k_F which is also seen in BHF calculations [47]. The peak reflects the increase of the level density due to the vanishing imaginary part of the optical potential at k_F which is also seen, e.g., in shell model calculations [45,17]. One has, however, to account for correlations beyond mean field or Hartree-Fock in order to reproduce this behavior. Fig. 8 com-

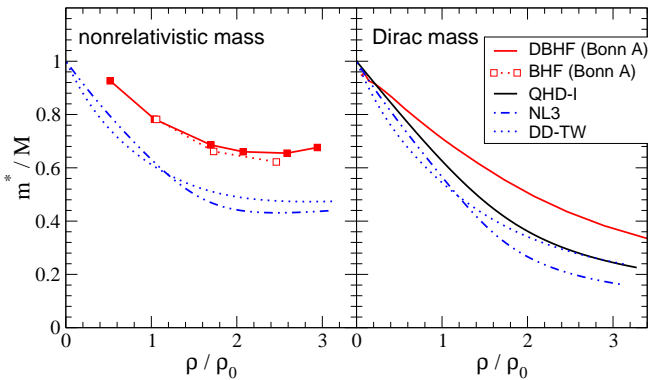


Fig. 8. Nonrelativistic and Dirac effective mass in isospin symmetric nuclear matter as a function of the density for various models.

pares the density dependence of the two effective masses determined at k_F . Both masses decrease with increasing density, the Dirac mass continuously, while m_{NR}^* starts to rise again at higher densities. Phenomenological density functionals (QHD-I, NL3, DD-TW) yield systematically smaller values of m_{NR}^* than the microscopic approaches. This reflects the lack of nonlocal contributions from short-range and many-body correlations in the mean field approaches.

3.1.1 Proton-neutron mass splitting

A heavily discussed topic is in the moment the proton-neutron mass splitting in isospin asymmetric nuclear matter. This question is of importance for the forthcoming new generation of radioactive beam facilities which are devoted to the investigation of the isospin dependence of the nuclear forces at its extremes. However, presently the predictions for the isospin dependences differ substantially. BHF calculations [18,47] predict a proton-neutron mass splitting of $m_{NR,n}^* > m_{NR,p}^*$. This stands in contrast to relativistic mean-field (RMF) theory. When only a vector isovector ρ -meson is included Dirac phenomenology predicts equal masses $m_{D,n}^* = m_{D,p}^*$ while the inclusion of the scalar isovector δ -meson, i.e. $\rho + \delta$, leads to $m_{D,n}^* < m_{D,p}^*$ [44]. When the effective mass is derived from RMF theory, it shows the same behavior as the corresponding Dirac mass, namely $m_{NR,n}^* < m_{NR,p}^*$ [44]. Conventional Skyrme forces, e.g. SkM*, lead to $m_{NR,n}^* < m_{NR,p}^*$ [49] while the more recent Skyrme-Lyon interactions (SkLya) predict the same mass splitting as RMF theory. The predictions from relativistic DBHF calculations are in the literature still controversial. They depend strongly on approximation schemes and techniques used to determine the Lorentz and the isovector structure of the nucleon self-energy. In the approach originally proposed by Brockmann and Machleidt [21] one extracts the scalar and vector self-energy components directly from the single-particle potential. Thus, by a fit to the single-particle potential mean values for the self-energy components are obtained where the explicit momentum-dependence has already been averaged out. In symmetric nuclear matter this method is relatively reliable but the extrapolation to asymmetric matter is ambiguous [24]. Calculations based on this method predict a mass splitting of $m_{D,n}^* > m_{D,p}^*$ [50]. On the other hand, the components of the self-energies can directly be determined from the projection onto Lorentz invariant amplitudes [20,22,23,24,26,51]. Projection techniques are involved but more accurate and yield the same mass splitting as found in RMF theory when the δ -meson is included, i.e. $m_{D,n}^* < m_{D,p}^*$ [22,24,26]. Recently also the non-relativistic effective mass has been determined with the DBHF approach and here a reversed proton-neutron mass splitting was found, i.e. $m_{NR,n}^* > m_{NR,p}^*$ [48]. Thus DBHF is in agreement with the results from nonrelativistic BHF calculations.

Experimentally accessible is the $p-n$ mass splitting, or the magnitude of the corresponding isovector effective mass m_V^* , ($\frac{\beta}{m_V^*} = \frac{\beta+1}{m_{NR}^*} - \frac{1}{m_{NR,n}^*}$) through the electric dipole photoabsorption cross section, i.e. through an enhancement of the Thomas-Reiche-Kuhn sum rule by the factor m/m_V^* . However, values derived from GDR measurements range presently from $m_V^*/m = 0.7 \div 1.05$ [46,52,53]. The forthcoming radioactive beam facilities will certainly improve on this not yet satisfying situation.

3.2 Optical potentials

The second important quantity related to the momentum dependence of the mean field is the optical nucleon-nucleus potential. At subnormal densities the optical potential U_{opt} is constraint by proton-nucleus scattering data [54] and at supra-normal densities constraints can be derived from heavy ion reactions [55,56,57]. In a relativistic framework the optical Schrödinger-equivalent nucleon potential (real part) is defined as

$$U_{\text{opt}} = -\Sigma_S + \frac{E}{M}\Sigma_V + \frac{\Sigma_S^2 - \Sigma_V^2}{2M} . \quad (6)$$

One should thereby note that in the literature sometimes also an optical potential, given by the difference of the single-particle energies in medium and free space $U = E - \sqrt{M^2 + \mathbf{k}^2}$ is used [55] which should be not mixed up with (6). In a relativistic framework momentum independent fields $\Sigma_{S,V}$ (as e.g. in RMF theory) lead always to a linear energy dependence of U_{opt} . As seen from Fig. 9 DBHF reproduces the empirical optical potential [54] extracted from proton-nucleus scattering for nuclear matter at ρ_0 reasonably well up to a laboratory energy of about 0.6-0.8 GeV. However, the saturating behavior at large momenta cannot be reproduced by this calculations because of missing inelasticities, i.e. the excitation of isobar resonances above the pion threshold. When such continuum excitations are accounted for optical model calculations are able to describe nucleon-nucleus scattering data also at higher energies [58]. In heavy ion reactions at incident energies above 1 AGeV such a saturating behavior is required in order to reproduce transverse flow observables [57]. One has then to rely on phenomenological approaches where the strength of the vector potential is artificially suppressed, e.g. by the introduction of additional form factors [57] or by energy dependent terms in the QHD Lagrangian [59] (D^3C model in Fig.9).

The isospin dependence, expressed by the isovector optical potential $U_{\text{iso}} = (U_{\text{opt},n} - U_{\text{opt},p})/(2\beta)$ is much less constrained by data. The knowledge of this quantity is, however, of high importance for the forthcoming radioactive beam experiments. The right panel of Fig. 9 compares the predictions from DBHF [26] and BHF [60] to the phenomenological Gogny and Skyrme (SkM* and SkLy) forces and a relativistic $T - \rho$ approximation [62] based on empirical NN scattering amplitudes [63]. At large momenta DBHF agrees with the tree-level results of [62]. While the dependence of U_{iso} on the asymmetry parameter β is found to be rather weak [26,60], the predicted energy and density dependences are quite different, in particular between the microscopic and the phenomenological approaches. The energy dependence of U_{iso} is very little constrained by data. The old analysis of optical potentials of scattering on charge asymmetric targets by Lane [64] is consistent with a decreasing potential as predicted by DBHF/BHF, while more recent analyses based on Dirac phenomenology [65] come to the opposite conclusions. RMF models show a linearly increasing energy dependence of U_{iso} (i.e. quadratic in k) like SkLy,

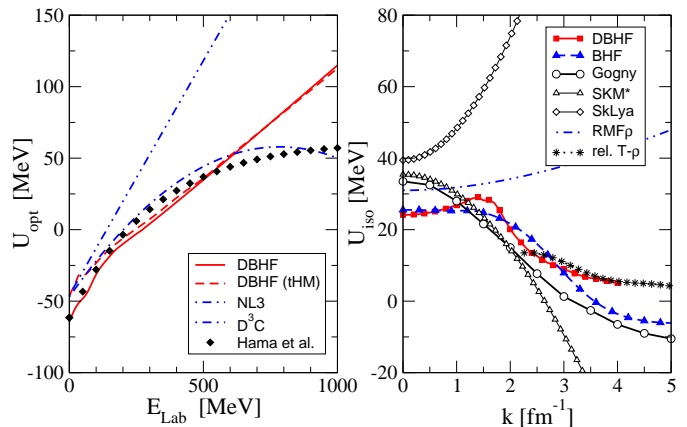


Fig. 9. Nucleon optical potential in nuclear matter at ρ_0 . On the left side DBHF calculations for symmetric nuclear matter from [20] and [23] are compared to the phenomenological models NL3 and D^3C [59] and to the p-A scattering analysis of [54]. The right panel compares the iso-vector optical potential from DBHF [26] and BHF [60] to phenomenological RMF [61], Gogny and Skyrme forces and to a relativistic $T - \rho$ approximation [62].

however generally with a smaller slope (see discussion in [44]). To clarify this question certainly more experimental efforts are necessary.

4 Transport models

The difficulty to extract information on the EOS from heavy ion reactions lies in the fact that the colliding system is over a large time span of the reaction out of global and even local equilibrium. At intermediate energies the relaxation time needed to equilibrate coincides more or less with the high density phase of the reaction. Hence, non-equilibrium effects are present all over the compression phase where one essentially intends to study the EOS at supra-normal densities. Experimental evidences for incomplete equilibration even in central collisions have been found by isospin tracing of projectile and target nuclei [66] and by different variances of longitudinal and transverse rapidity distributions [67]. To account for the temporal space time evolution of the reactions requires dynamical approaches which are based on kinetic transport theory. In the following we briefly discuss the various approaches which are mainly used in order to describe the reaction dynamics at low and intermediate energies.

4.1 Boltzmann-type kinetic equations

The theoretical basis for the description of the collision dynamics at energies ranging from the Fermi regime up to 1-2 AGeV is hadronic non-equilibrium quantum transport field theory [68]. The starting point of non-equilibrium QFT is the Schwinger-Keldysh formalism for many-body Green functions in non-equilibrium configurations. The one-body Green function is defined as the expectation

value of the time ordered product of fermionic field operators $G(1, 1') = (-i) \langle \mathcal{T}_{sk}(\Psi(1)\bar{\Psi}(1')) \rangle$ where \mathcal{T}_{sk} defines the temporal sequence of the field operators. In non-equilibrium time reversal invariance is violated and thus the application of \mathcal{T}_{sk} leads to four possible combinations [68]:

$$\begin{aligned} G^c &= -i\langle T^c[\Psi(1)\bar{\Psi}(1')]\rangle, \quad G^a = -i\langle T^a[\Psi(1)\bar{\Psi}(1')]\rangle, \\ G^> &= -i\langle \Psi(1)\bar{\Psi}(1')\rangle, \quad G^< = i\langle \bar{\Psi}(1')\Psi(1)\rangle \end{aligned} \quad (7)$$

where T^c (T^a) is the causal (anti-causal) time ordering operator. The physical quantity of interest is the correlation function $G^<$ since it corresponds in the equal time limit to the density $\lim_{t_1, t_1' \rightarrow t_1} G^<(1, 1') = (+i)\rho(\mathbf{x}_1, \mathbf{x}_1', t)$. However, the four Green-functions are related through equations of motion (Kadanoff-Baym Equations) for the correlation $G^{<, >}$ and the retarded and advanced G^\pm functions (the retarded and advanced Green functions are defined via $G^{+, -} = G^c - G^{<, >} = G^>, < - G^a$). From the Kadanoff-Baym Eqs. one obtains a kinetic equation for the correlation function $G^<$

$$\begin{aligned} DG^< - G^< D^* - (Re\Sigma^+ G^< - G^< Re\Sigma^+) - (\Sigma^< ReG^+ \\ - ReG^+ \Sigma^<) = \frac{1}{2} (\Sigma^> G^< + G^< \Sigma^> - \Sigma^< G^> - G^> \Sigma^<) \end{aligned} \quad (8)$$

$D = -i\partial_{x_1}/2M$ is the Schrödinger operator or in a relativistic framework the Dirac operator ($D = i\gamma_\mu\partial_{x_1} - M$) and $\Sigma^{<, >, \pm}$ are the self energies. The introduction of retarded and advanced functions allows to interpret the real part of the retarded self energy as a mean field while the imaginary part describes the absorption or finite life times of quasi particles (dressed nucleons) [68]. The self-energy Σ contains all higher order correlations and couples the one-body kinetic equation (8) to the corresponding equations for the two- and 3-body densities and so forth. This requires to truncate the Dyson-Schwinger hierarchy which is usually done at the two-body level and leads to the ladder approximation for T-matrix, i.e. the Bethe-Salpeter equation.

The formal structure of the kinetic equation (8) is complex and one should solve (8) together with the corresponding kinetic equations for G^\pm which describe the *spectral properties* of the phase space distribution. Simultaneously the self-energies should be derived for arbitrary non-equilibrium situations [68]. A solution of the full self-consistency problem has not yet achieved. In praxis one applies further approximations. The most important ones are the *gradient expansion* (a semi-classical approximation to first order in \hbar) and the *quasi-particle approximation* which sets the particles on mass shell. The result is a Boltzmann-type transport equation, which is known as the Boltzmann-Uheling-Uhlenbeck (BUU) transport equation [69]. In its relativistic form the (R)BUU equation reads

$$\begin{aligned} &[(m_D^* \partial_x^\mu m_D^* - k^* \nu \partial_x^\mu k_\nu^*) \partial_\mu^k - (m_D^* \partial_k^\mu m_D^* - k^* \nu \partial_k^\mu k_\nu^*) \partial_\mu^x] f \\ &= \frac{1}{2(2\pi)^8} \int \frac{d^3 k_2}{E_{k_2}^*} \frac{d^3 k_3}{E_{k_3}^*} \frac{d^3 k_4}{E_{k_4}^*} W \delta^4(k + k_2 - k_3 - k_4) \\ &\times \left[f_3 f_4 (1-f)(1-f_2) - f f_2 (1-f_3)(1-f_4) \right] , \quad (9) \end{aligned}$$

which describes the phase space evolution of the 1-particle distribution $f(\mathbf{x}, \mathbf{k}, t)$ under the influence of the mean field (which enters via the real part of the self energy, i.e. via $m_D^* = M - \Sigma_S$ and $k^{*\mu} = k^\mu - \Sigma^\mu$) and binary collisions determined by the transition amplitude $W = m_D^{*4} |T(k_2|k_3 k_4)|^2$. Final state Pauli blocking is accounted for by the blocking factors $(1-f_i)$ in (9) with $f_i = f(\mathbf{x}, \mathbf{k}_i, t)$. The physical parameters entering into the kinetic equation are the mean field, i.e. the nuclear EOS, and elementary cross sections for 2-particle scattering processes. Thus one can test the high density behavior of the nuclear EOS in heavy ion collisions and the in-medium modifications of cross sections, which also influence the stopping properties of the colliding system. Above the pion threshold where inelastic processes start to play an important role the Eq. (9) becomes a *coupled channel* problem for nucleonic, nucleon resonance and mesonic degrees of freedom. The collision integral, i.e. the right hand side of Eq. (9) has to be extended for the corresponding inelastic and absorptive processes and the new degrees of freedom must be propagated in their mean fields. In practice the transport equation is solved within the *testparticle method* which describes the phase space distribution f as an incoherent sum of point-like quasi particles [69] or static gaussians [70] which propagate on classical trajectories. Relativistic formulations of the two methods were developed in [71] and [72].

4.2 Quantum Molecular Dynamics (QMD)

An alternative approach to the kinetic BUU equation is Quantum Molecular Dynamics (QMD) [73,74,75]. QMD is a N-body approach which simulates heavy ion reactions on an event by event basis taking fluctuations and correlations into account. The QMD equations are formally derived from the assumption that the N-body wave function Φ can be represented as the direct product of single coherent states $\Phi = \prod_i \phi_i$ which are described by Gaussian wave packets. Anti-symmetrization is *not* taken into account. A Wigner transformation yields the corresponding phase space representation of Φ . The equations of motion of the many-body system are obtained by the variational principle starting from the action $S = \int \mathcal{L}[\Phi, \Phi^*]$ (with the Lagrangian functional $\mathcal{L} = \langle \Phi | i\hbar \frac{d}{dt} - H | \Phi \rangle$). The Hamiltonian H contains a kinetic contribution and mutual two-body interactions V_{ij} . The variational principle leads finally to classical equations of motion for the generalized coordinates \mathbf{q}_i and \mathbf{k}_i of the Gaussian wave packets

$$\begin{aligned} \dot{\mathbf{q}}_i &= \frac{\mathbf{k}_i}{m} + \nabla_{\mathbf{k}_i} \sum_{j \neq i} \langle V_{ij} \rangle = \nabla_{\mathbf{k}_i} \langle H \rangle , \\ \dot{\mathbf{k}}_i &= -\nabla_{\mathbf{q}_i} \sum_{j \neq i} \langle V_{ij} \rangle = \nabla_{\mathbf{q}_i} \langle H \rangle . \end{aligned}$$

The two-body interaction V_{ij} can be e.g. taken from BHF calculations [75] or from local Skyrme forces which are usually supplemented by an empirical momentum dependence in order to account for the energy dependence of the

optical nucleon-nucleus potential [73]. Binary collisions are treated in the same way as in BUU models. Furthermore there exist relativistic extensions, i.e. RQMD and the UrQMD model which has been developed to simulate heavy ion collisions at ultra-relativistic energies [74,76].

4.3 Antisymmetrized Molecular Dynamics (AMD/FMD)

An extension of QMD, in particular designed for low energies, are the Antisymmetrized Molecular Dynamics (AMD) [77] and Fermionic Molecular Dynamics (FMD) approaches [78]. In contrast to conventional QMD, the interacting system is represented by an *antisymmetrized* many-body wave function consisting of single-particle states which are localized in phase space. The equations of motion for the parameters characterizing the many-body state (e.g. position, momentum, width and spin of the particles) are derived from a quantum variational principle. The models are designed to describe ground state properties of nuclei as well as heavy ion reactions at low energies (see also Chap. I.2).

4.4 Off-shell transport

Essential for the validity of the classical equations of motion is the quasi-particle approximation (QPA) which assumes that the spectral strength of a hadron is concentrated around its quasi-particle pole. Particle widths can, however, dramatically change in a dense hadronic environment. To first order in density the in-medium width of a hadron in nuclear matter can be estimated by the collision width $\Gamma^{\text{tot}} = \Gamma^{\text{vac}} + \Gamma^{\text{coll}}$, $\Gamma^{\text{coll}} = \gamma v \sigma \rho_B$ with v the hadron velocity relative to the surrounding matter and σ the total hadron-nucleon cross section. A consistent treatment of the off-shell dynamics, i.e. a solution of the quantum evolution equations for the correlation functions $G^{<,>}$ has up to now only been performed for toy models and simplified geometries [79,80] or in first order gradient approximation leading to an extended quasi-particle picture [81]. Comparing the nonlocal extension of BUU with standard simulations a visible effect of nonlocal correlations is seen and a better agreement with measured charge density distribution [82] or particle spectra [83] due to the virial corrections has been found. To develop a consistent lattice quantum transport for non-uniform systems and realistic interactions will be one of the future challenges in theoretical heavy ion physics.

On the other hand, substantial progress has been made in the recent years to map part of the off-shell dynamics on a modified test-particle formalism [84,85]. This allows to apply off-shell dynamics, although in a simplified form, to the complex space time evolution of a heavy ion reaction. The present knowledge of off-shell matrix elements is, however, rather limited and theoretical investigations are scarce [86]. The off-shell T-matrix has been used in order to calculate the duration and non-locality of a nucleon-nucleon collision [87]. The question to what

degree a depletion of the Fermi surface due to particle-hole excitations and the high momentum tails of the nuclear spectral functions will affect subthreshold particle production is not so obvious to answer. The high momentum tails correspond to deeply bound states which are off-shell and to treat such states in a standard transport approach like on-shell quasi-particles would violate energy-momentum conservation. Energy-momentum conservation can be achieved consistently by the nonlocal kinetic theory [88] taking into account first order off-shell effects. The contribution of the nuclear short-range correlations to subthreshold K^+ production in p+A reactions have e.g. been estimated in [89]. The removal energy for a high momentum state compensates the naively expected energy gain and the short-range correlations do therefore not significantly contribute to subthreshold particle production [89]. The situation changes, however, when the medium is heated up and high momentum particles become on-shell or when the spectral distributions of the produced hadrons themselves are broadened.

5 Constraints from heavy ion collisions

5.1 Flow and stopping

One of the most important observable to constrain the nuclear forces and the underlying EOS at supra-normal densities is the collective nucleon flow [90]. It can be characterized in terms of anisotropies of the azimuthal emission pattern. Expressed in terms of a Fourier series

$$\frac{dN}{d\phi} \propto 1 + 2v_1 \cos(\phi) + 2v_2 \cos(2\phi) + \dots \quad (10)$$

this allows a transparent interpretation of the coefficients v_1 and v_2 . The dipole term v_1 arises from a collective side-ward deflection of the particles in the reaction plane and characterizes the transverse flow in the reaction plane. The second harmonics describes the emission pattern perpendicular to the reaction plane. For negative v_2 one has a preferential out-of-plane emission. The phenomenon of an out-of-plane enhancement of particle emission at midrapidity is called *squeeze-out*.

The transverse flow v_1 has been found to be sensitive to the EOS and, in particular in peripheral reactions, to the momentum dependence of the mean field [55,56]. The elliptic flow v_2 , in contrast, is very sensitive to the maximal compression reached in the early phase of a heavy ion reaction. The cross over from preferential in-plane flow $v_2 < 0$ to preferential out-of-plane flow $v_2 > 0$ around 4-6 AGeV has also led to speculations about a phase transition in this energy region which goes along with a softening of the EOS [91]. The present situation between theory and experiment is illustrated in Fig. 10 (from [92]). The BUU studies from Danielewicz et al. and the Giessen group (Larionov et al.) investigated the EOS dependence while Persson et al. find a sensitivity of v_2 on the medium dependence of the NN cross sections. Finally, non-equilibrium effects

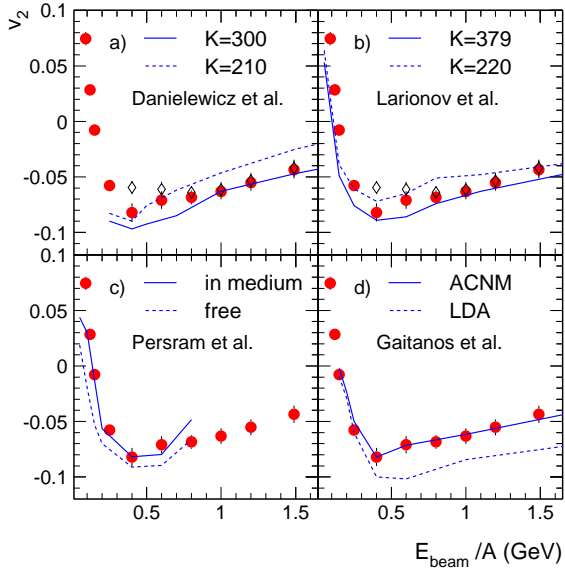


Fig. 10. Elliptic flow excitation function at SIS energies. Various theoretical studies using different EOS's ((a),(b)), or different cross sections (c) or DBHF mean fields in the LDA approach and including further non-equilibrium effects (ACNM) are compared to FOPI data (symbols). Figure is taken from [92].

have been investigated at the level of the effective interaction in [56,93]. It has been found that the local phase space anisotropies of the pre-equilibrium stages of the reactions reduce the repulsion of the mean field and soften the corresponding EOS which allows a good description of the v_2 data using microscopic DBHF mean fields (Gaitanos et al.). However, Fig. 10 also demonstrates that v_2 is generated by the interplay of the mean field and binary collisions which makes it difficult to extract exclusive information on the EOS from the data. Here certainly further going studies are required.

The next figure 11, based on the studies of Danielewicz [94], summarizes the status obtained within this model in terms of a band that represents the constraints from collective flow data. It is based on a compilation from the analysis of sideward and elliptic anisotropies, ranging from low SIS ($E_{\text{lab}} \simeq 0.2 \div 2$ AGeV) up to top AGS energies ($E_{\text{lab}} \simeq 2 \div 11$ AGeV), has been studied in [94]. The conclusion from this study was that, both, super-soft equations of state ($K=167$ MeV) as well as hard EOSs ($K>300$ MeV) are ruled out by data. At SIS energies existing flow data are consistent with a soft EOS [95,55], e.g. the soft Skyrme EOS. In the models used by Danielewicz et al. [55,94] sideward flow favors a rather soft EOS with $K=210$ MeV while the development of the elliptic flow requires slightly higher pressures. The BHF and variational calculations including 3-body-forces³ fit well into

the constrained area up to $4\rho_0$. At higher densities the microscopic EOSs, also DBHF, tend to be too repulsive. However, conclusions from flow data are generally com-

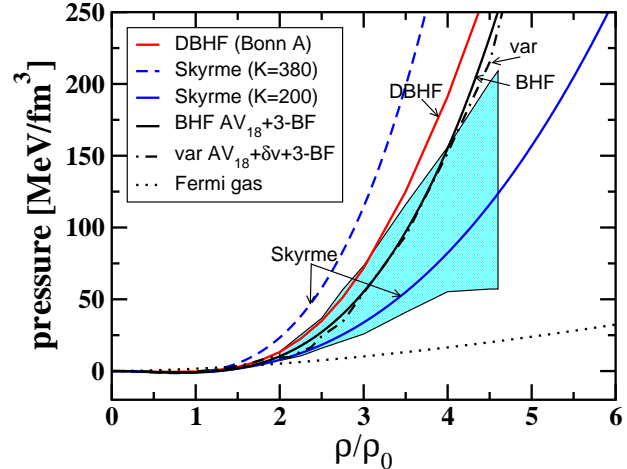


Fig. 11. Constraints on the nuclear EOS from heavy ion flow data. The shaded area shows the pressure-density which is compatible with heavy ion flow data according the analysis on [94]. The equations-of-state from the models shown in Fig. 3 are displayed.

plicated by the interplay of the compressional part of the nuclear EOS and the momentum dependence of the nuclear forces. A detailed comparison to v_1 and v_2 data from FOPI [96,97] and KaoS [98] for v_1 and v_2 below 1 AGeV favors again a relatively soft EOS with a momentum dependence close to that obtained from microscopic DBHF calculations [55,56,99]. In Fig. 11 the microscopic DBHF EOS ($K=230$ MeV) lies at the upper edge of the boundary, but is still consistent in the density range tested at SIS energies, i.e. up to maximally $3\rho_0$. This fact is further consistent with the findings of Gaitanos et al. [56,99] where a good description of v_1 and v_2 data at energies between 0.2 and 0.8 AGeV has been found in RBUU calculations based on DBHF mean fields. As pointed out in [56,93,99] it is thereby essential to account for non-equilibrium effects and the momentum dependence of the forces which softens the EOS compared to the equilibrium case (shown in Fig. 11).

As can be seen from Fig. 10, not only the nuclear EOS, but also the cross sections for elementary 2-particle scattering influences the collective dynamics, in particular the degree of stopping and hence the maximal compression achieved in the fireball region. A challenge is in this context the quantitative understanding of the recently observed strong correlations between maximal side flow v_1 and maximal stopping in both excitation functions [67] (see Chap. I.5 by W. Reisdorf et al.). Most collective flow analyses performed so far have been based on free cross sections, which works astonishingly well from a practical point of view. However, within a consistent picture

³ For the BHF + 3-BF calculation the pressure shown in Fig. 11 has been determined from the parameterization given in [19]

which is based on the Urbana IX 3-BF different to that used in [18].

one should treat the in-medium effects in both, real (nuclear EOS) and the imaginary part (cross sections) of the interaction on the same footing. Many-body calculations (BHF/DBHF) predict an essential reduction of the elastic NN cross section with increasing baryon density [75,100,86] and in [101] a similar reduction was proposed for the inelastic channels in order to describe pion multiplicities in the 1-2 AGeV region. One can therefore expect observable signals in heavy ion collisions. In fact, recent QMD studies of stopping and transparency observables have shown that the data can be reproduced when the free cross section is reduced by a factor of 0.5 [102]. These findings are supported by transport calculations using microscopic in-medium cross sections [103,104]. Therefore, for a reliable extraction of the high density nuclear EOS one should account for in-medium effects not only in the potential, but also in the cross sections.

5.1.1 Isospin dependence of the EOS

Another important aspect of heavy ion collisions is the investigation of the density dependence of the EOS for asymmetric matter. There exist abundant studies on this sector, either non-relativistically or relativistically.

The momentum dependence of the isovector potential, Fig. 9, which is also closely related to the proton/neutron mass splitting of both, the non-relativistic m_{NR}^* and the Dirac m_D^* effective mass, is one of the key questions which can be addressed by nuclear reactions induced by neutron-rich nuclei at RIA energies. Transverse and elliptic flow pattern as well p/n rapidity distributions have been suggested as possible observables to investigate the momentum dependence and the p/n mass splitting [105,106,107].

Promising observables to pin down the density dependence of the symmetry energy are the iso-scaling behavior of fragment yields and the isospin diffusion in asymmetric colliding systems. In both cases recent NSCL-MSU data in combination with transport calculations are consistent with a value of $E_{\text{sym}} \approx 31$ at ρ_0 and rule out extremely "stiff" and "soft" density dependences of the symmetry energy [108,109] (see also Chap. III.2). The same value has been extracted [110] from low energy elastic and (p,n) charge exchange reactions on isobaric analog states, i.e. $p(^6He, ^6Li^*)n$ measured at the HMI. Such a behavior is also consistent with the predictions from many-body theory [15,26]. Also the p/n ratio at mid-rapidity has been found to be sensitive to the high density behavior of nuclear symmetry energy [111].

In relativistic approaches large attractive scalar and repulsive vector fields are required by Dirac phenomenology in order to describe simultaneously the central potential and the strong spin-orbit force in finite nuclei [8,9,12]. The situation is, however, less clear in the iso-vector sector. There exists different possibilities to reproduce the same value of the a_4 coefficient (4): (a) by only an iso-vector vector ρ field like in most RMF models (NL3 etc.), or (b) by accounting for an additional iso-vector scalar δ field. Due to competing effects between attractive (scalar δ) and repulsive (vector ρ) both alternatives can be fitted

to the same empirical a_4 parameter, but the inclusion of δ field leads to an essentially different high density behavior of the symmetry energy [112]. The scalar δ field is suppressed at high densities, whereas the vector field is proportional to the baryon density which makes the symmetry stiffer energy at supra-normal densities. Recent transport studies have shown that these subtle relativistic effects can be observed in the intermediate energy range by means of collective isospin flow, particle ratios and imbalance ratios of different particle species (protons, neutrons, pions and kaons) [112,107,44]. However, due to the lack of precise experimental data no definitive conclusions could be made so far.

5.2 Particle production

5.2.1 Pions

With the start of the first relativistic heavy ion programs the hope was that particle production would provide a direct experimental access to nuclear EOS [113]. At two times saturation density which is reached in the participant zone of the reactions without additional compression the difference between the soft and hard EOS shown in Fig. 3 is about 13 MeV in binding energy. If the matter is compressed up to $3\rho_0$ the difference is already ~ 55 MeV. It was expected that the compressional energy should be released into the creation of new particles, primarily pions, when the matter expands [113]. However, pions have large absorption cross sections and they turned out not to be suitable messengers of the compression phase. They undergo several absorption cycles through nucleon resonances ($N\pi \leftrightarrow \Delta$) and freeze out at final stages of the reaction and at low densities. Hence pions loose most of their knowledge on the compression phase and are not really sensitive probes for stiffness of the EOS [114]. However, they carry information on the isotopic composition of the matter which is to some extent conserved until freeze-out. The final π^-/π^+ ratio was found to be sensitive to the initial n/p composition of the matter which, on the other hand, is influenced by the isospin dependence of the nuclear forces [115,116]. In [61] a reduction of the π^-/π^+ -ratio was found when the δ -meson was included in the RMF approach. The effects are, however, moderate, i.e. at the 10-20% level, and most pronounced at extreme phase space regions, e.g. at the high energy tails of p_t spectra [116,61,117]. Systematic measurements, e.g. from the FOPI Collaboration may help to constrain the isospin dependence by pionic observables.

5.2.2 Kaons

After pions turned out to fail as suitable messengers, K^+ mesons were suggested as promising tools to probe the nuclear EOS, almost 20 years ago [119]. The cheapest way to produce a K^+ meson is the reactions $NN \rightarrow N\Lambda K^+$ which has a threshold of $E_{\text{lab}} = 1.58$ GeV kinetic energy for the incident nucleon. When the incident energy per

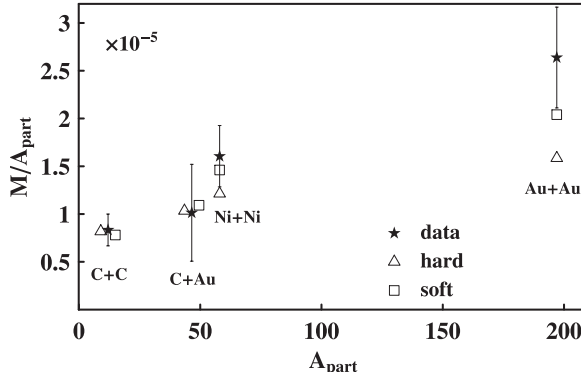


Fig. 12. K^+ multiplicities in inclusive C+C, Ni+Ni, Au+Au and C+Au reactions at 1 AGeV. QMD calculations using a hard/soft nuclear EOS are compared to KaoS data [118]. Figure is taken from [118].

nucleon in a heavy ion reactions is below this values one speaks about *subthreshold* kaon production. Subthreshold kaon production is in particular interesting since it ensures that the kaons originate from the high density phase of the reaction. The missing energy has to be provided either by the Fermi motion of the nucleons or by energy accumulating multi-step reactions. Both processes exclude significant distortions from surface effects if one goes sufficiently far below threshold. In combination with the long mean free path subthreshold K^+ production is an ideal tool to probe compressed nuclear matter in relativistic heavy ion reactions.

Already in the first theoretical investigations by transport models it was noticed the K^+ yield reacts rather sensitive on the EOS [120,121,122]. Both, in non-relativistic QMD calculations based on soft/hard Skyrme forces [120,121] and in RBUU [122,124] with soft/hard versions of the (non-linear) $\sigma\omega$ -model the K^+ yield was found to be about a factor 2–3 larger when a soft EOS is applied compared to a hard EOS. At that time the available data favored a soft equation of state [121,122,124]. However, at that stage the theoretical calculations were still burdened with large uncertainties. First of all, it was noticed [120,121] that the influence of the repulsive momentum dependent part of the nuclear interaction leads to a strong suppression of the kaon abundances which made a quantitative description of the available data more difficult. Moreover, at that time the pion induced reaction channels $\pi B \rightarrow Y K^+$ have not yet been taken into account. These additional channels which contribute up to 30 \div 50% to the total yield enabled to explain the measured yields with realistic momentum dependent interactions [123,125]. A breakthrough was achieved when the COSY-11 Collaboration measured the $pp \rightarrow p K^+ \Lambda$ reactions at threshold [126] which constrains the strangeness production cross sections $NN \rightarrow NK^+Y$. Within the last decade the KaoS Collaboration has performed systematic measurements of the K^+ production far below threshold [114,127,128]. Based on the new data situation, the question if valuable information on the nuclear EOS can be extracted has been revisited and it has been shown that subthreshold K^+

production provides indeed a suitable and reliable tool for this purpose [129,130,131].

Fig. 12 compares measured the K^+ multiplicities as a function of participating nucleons A_{part} in Au+Au, Ni+Ni, C+Au and C+C reactions at 1 AGeV to QMD calculation using a soft/hard momentum dependent Skyrme force [118]. This figure demonstrates thereby the interplay between A_{part} , system size and EOS. A significant dependence of the kaon multiplicities on the nuclear EOS requires a large amount of collectivity which is easiest reached in central reactions of heavy mass systems. Consequently, the EOS dependence is most pronounced in central Au+Au reactions. Also in Ni+Ni effects are still sizable while the small C+C system is completely insensitive on the nuclear EOS even in most central reactions. The data available for Au+Au and Ni+Ni support the soft EOS. Interesting is in this context the asymmetric C+Au system: Though in central C+Au reactions the number of participants is comparable to Ni+Ni the K^+ yield does not depend on the EOS. This indicates again that a sensitivity on the EOS is not only a question of A_{part} but of the compression which can be reached by the colliding system. The next step is to consider now the energy

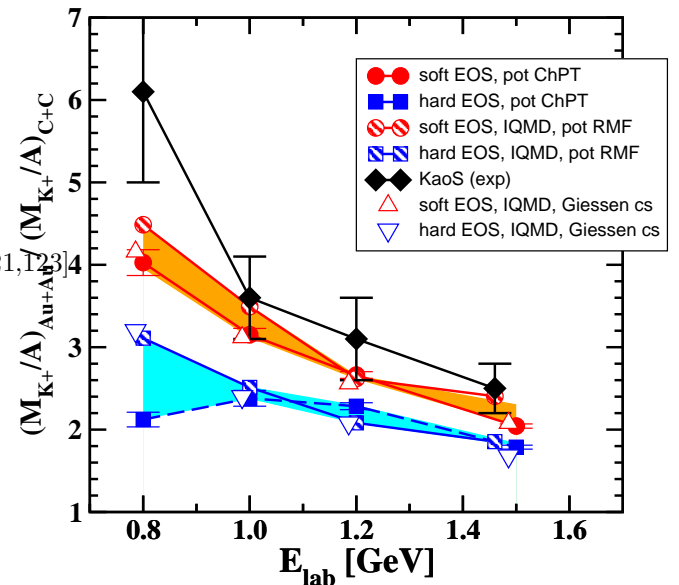


Fig. 13. Excitation function of the ratio R of K^+ multiplicities obtained in inclusive Au+Au over C+C reactions. QMD [130] and IQMD calculations [131] are compared to the KaoS data [128]. The shaded area indicates thereby the range of uncertainty in the theoretical models. In addition IQMD results based on an alternative set of elementary K^+ production cross sections are shown.

dependence of the EOS effect. It is expected to be most pronounced most far below threshold because there the highest degree of collectivity, reflected in multi-step collisions, is necessary to overcome the production thresholds. The effects become even more evident when the ratio R of the kaon multiplicities obtained in Au+Au over C+C re-

actions (normalized to the corresponding mass numbers) is built [130,128]. Such a ratio has moreover the advantage that possible uncertainties which might still exist in the theoretical calculations should cancel out to large extent. This ratio is shown in Fig. 13. Both, soft and hard EOS, show an increase of R with decreasing energy. However, this increase is much less pronounced when the stiff EOS is employed. The strong increase of R can be directly related to higher compressible nuclear matter. The comparison to the experimental data from KaoS [128] where the increase of R is even more pronounced strongly favors a soft equation of state. These findings were confirmed by independent IQMD transport calculations of the Nantes group [131]. Both, QMD and IQMD included also a repulsive kaon-nucleon potential as predicted by chiral perturbation theory [129]. The shaded area in the figure can be taken as the existing range of uncertainty in the theoretical model description of the considered observable. To estimate the stability of the conclusions the IQMD calculations have been repeated with an alternative set of $N\Delta; \Delta\Delta \rightarrow NYK^+$ cross sections⁴ which are almost one order of magnitude smaller than those used originally, but the EOS dependence remained stable [132].

6 Constraints from neutron stars

Measurements of “extreme” values, like large masses or radii, huge luminosities etc. as provided by compact stars offer good opportunities to gain deeper insight into the physics of matter under extreme conditions. There has been substantial progress in recent time from the astrophysical side.

The most spectacular observation was probably the recent measurements on PSR J0751+1807, a millisecond pulsar in a binary system with a helium white dwarf secondary, which implies a pulsar mass of 2.1 ± 0.2 ($^{+0.4}_{-0.5}$) M_\odot with 1σ (2σ) confidence [133]. Therefore a reliable EOS has to describe neutron star (NS) masses of at least $1.9 M_\odot$ (1σ) in a strong, or $1.6 M_\odot$ (2σ) in a weak interpretation. This condition limits the softness of EOS in NS matter. One might therefore be worried about an apparent contradiction between the constraints derived from neutron stars and those from heavy ion reactions. While heavy ion reactions favor a soft EOS, PSR J0751+1807 requires a stiff EOS. The corresponding constraints are, however, complementary rather than contradictory. Intermediate energy heavy ion reactions, e.g. subthreshold kaon production, constrains the EOS at densities up to $2 \div 3 \rho_0$ while the maximum NS mass is more sensitive to the high density behaviour of the EOS. Combining the two constraints implies that the EOS should be *soft at moderate densities and stiff at high densities*. Such a behaviour is predicted by microscopic many-body calculations (see Fig. 3). DBHF, BHF or variational calculations lead typically the maximal NS masses between $2.1 \div 2.3 M_\odot$ and are therefore in accordance with PSR J0751+1807 [134].

⁴ Cross section which involve Δ resonances in the initial of final states are not constrained by measurements.

There exist several other constraints on the nuclear EOS which can be derived from observations of compact stars, see e.g. [134,135,136]. Among these the one of the most promising constraints is the Direct Urca (DU) process which is essentially driven by the proton fraction inside the NS [137]. DU processes, e.g. the neutron β -decay $n \rightarrow p + e^- + \bar{\nu}_e$, are very efficient regarding their neutrino production, even in superfluid NM [138,139], and cool NSs too fast to be in accordance with data from thermal observable NSs. Therefore one can suppose that no DU processes should occur below the upper mass limit for “typical” NSs, i.e. $M_{DU} \geq 1.5 M_\odot$ ($1.35 M_\odot$ in a weak interpretation). These limits come from a population synthesis of young, nearby NSs [140] and masses of NS binaries [133].

7 Summary and outlook

The quest for the nuclear equation of state is one of the longstanding problems in physics which has a more than 50 years history in nuclear structure. Since about 30 years one tries to attack this question with heavy ion reactions. The exploration of the limits of stability, i.e. the regimes of extreme isospin asymmetry, is a relatively new field with rapidly growing importance in view of the forthcoming generation of radioactive beam facilities.

The status of theoretical models which make predictions for the EOS can roughly be summarized as follows: phenomenological density functionals such as Skyrme, Gogny or relativistic mean field models provide high precision fits to the nuclear chart but extrapolations to supra-normal densities or the limits of stability are highly uncertain. A more controlled way provide effective field theory approaches which became quite popular in recent time. Effective chiral field theory allows e.g. a systematic generation of two- and many-body nuclear forces. However, these approaches are low momentum expansions and when applied to the nuclear many-body problem, low density expansions. Ab initio calculations for the nuclear many-body problem such as variational or Brueckner calculations have reached a high degree of sophistication and can serve as guidelines for the extrapolation to the regimes of high density and/or large isospin asymmetry. Possible future developments are to base such calculations on modern EFT potentials and to achieve a more consistent treatment of two- and three-body forces.

If one intends to constrain these models by nuclear reactions one has to account for the reaction dynamics by semi-classical transport models of a Boltzmann or molecular dynamics type. Suitable observables which have been found to be sensitive on the nuclear EOS are directed and elliptic collective flow pattern and particle production, in particular kaon production, at higher energies. Heavy ion data suggest that the EOS of symmetric nuclear matter shows a soft behavior in the density regime between one to about three times nuclear saturation density, which is consistent with the predictions from many-body calculations. Conclusions on the EOS are, however, complicated by the

interplay between the density and the momentum dependence of the nuclear mean field. Data which constrain the isospin dependence of the mean field are still scarce. Promising observables are isospin diffusion, iso-scaling of intermediate mass fragments and particle ratios (π^+/π^- and eventually K^+/K^0). Here the situation will certainly improve when the forthcoming radioactive beam facilities will be operating. This will also allow to measure the optical isospin potential in p+A and A+A reactions and to obtain more information of the symmetry energy and the proton/neutron mass splitting in asymmetric matter. From the theoretical side it will be unavoidable to invest significant efforts towards the development of quantum transport models with consistent off-shell dynamics.

We would like to thank K. Morawetz, T. Gaitanos and M. di Toro for fruitful discussions.

References

1. GSI Conceptual Design Report, <http://www.gsi.de/GSI-Future>
2. RIA homepage, <http://www.orau.org/ria>
3. H.A. Gustafsson *et al.*, Phys. Rev. Lett. **52**, 1590 (1984).
4. J. Decharge, D. Gogny, Phys. Rev. C **21**, 1568 (1980).
5. M. Kleban, B. Nerlo-Pomorska, J. F. Berger, J. Decharge, M. Girod, S. Hilaire, Phys. Rev. C **65**, 024309 (2002).
6. B. Cochet, K. Bennaceur, J. Meyer, P. Bonche, T. Duguet, Int. J. Mod. Phys. **E13**, 187 (2004).
7. P.-G. Reinhard, M. Bender, Lect. Notes Phys. **641**, 249 (2004).
8. P. Ring, Prog. Part. Nucl. Phys. **73**, 193 (1996); Lect. Notes Phys. **641**, 175 (2004).
9. B.D. Serot, J.D. Walecka, Int. J. Mod. Phys. **E6**, 515 (1997).
10. R.J. Furnstahl, Lect. Notes Phys. **641**, 1 (2004).
11. M. Lutz, B. Friman, Ch. Appel, Phys. Lett. B **474**, 7 (2000).
12. P. Finelli, N. Kaiser, D. Vretenar, W. Weise, Eur. Phys. J. A **17**, 573 (2003); Nucl. Phys. A **735**, 449 (2004).
13. D. Vretenar, W. Weise, Lect. Notes Phys. **641**, 65 (2004).
14. V.R. Pandharipande, R.B. Wiringa, Rev. Mod. Phys. **51**, 821 (1979).
15. A. Akmal, V.R. Pandharipande, D.G. Ravenhall, Phys. Rev. C **58**, 1804 (1998).
16. K.A. Brueckner, J.L. Gammel, Phys. Rev. **107**, 1023 (1958).
17. M. Jaminon, C. Mahaux, Phys. Rev. C **40**, 354 (1989).
18. W. Zuo, A. Lejeune, U. Lombardo, J.F. Mathiot, Nucl. Phys. A **706**, 418 (2002).
19. X.R. Zhou, G.F. Burgio, U. Lombardo, H.-J. Schulze, W. Zuo, Phys. Rev. C **69**, 018801 (2004).
20. B. ter Haar, R. Malfliet, Phys. Rep. **149**, 207 (1987).
21. R. Brockmann, R. Machleidt, Phys. Rev. C **42**, 1965 (1990).
22. F. de Jong, H. Lenske, Phys. Rev. C **58**, 890 (1998).
23. T. Gross-Boelting, C. Fuchs, A. Faessler, Nucl. Phys. A **648**, 105 (1999).
24. E. Schiller, H. Müther, Eur. Phys. J. **A11**, 15 (2001).
25. C. Fuchs, Lect. Notes Phys. **641**, 119 (2004).
26. E. van Dalen, C. Fuchs, A. Faessler, Nucl. Phys. A **744**, 227 (2004); Phys. Rev. C **72**, 065803 (2005).
27. H. Müther, A. Polls, Prog. Part. Nucl. Phys. **45**, 243 (2000).
28. W.H. Dickhoff, C. Barbieri, Prog. Part. Nucl. Phys. **52**, 377 (2004).
29. J. Carlson, J. Morales, V.R. Pandharipande, D.G. Ravenhall, Phys. Rev. C **68**, 025802 (2003).
30. B. D. Serot, J. D. Walecka, Adv. Nucl. Phys. **16**, 1 (1986).
31. J. Boguta, Phys. Lett. B **109**, 251 (1982).
32. C. Fuchs, H. Lenske, H. H. Wolter, Phys. Rev. C **52**, 3043 (1995); H. Lenske, C. Fuchs, Phys. Lett. B **345**, 355 (1995).
33. F. Hofmann, C.M. Keil, H. Lenske Phys. Rev. C **64**, 034314 (2001); C.M. Keil, F. Hofmann, H. Lenske Phys. Rev. C **61**, 064309 (2000).
34. S. Typel, H.H. Wolter, Nucl. Phys. A **656**, 331 (1999).
35. T. Nikšić, D. Vretenar, P. Ring, Phys. Rev. C **66**, 064302 (2002).
36. R. Machleidt, K. Holinde, Ch. Elster, Phys. Rep. **149**, 1 (1987).
37. M.K. Banerjee, J.A. Tjon, Phys. Rev. C **58**, 2120 (1998), Nucl. Phys. A **708**, 303 (2002).
38. U. van Klock, Phys. Rev. C **49**, 2932 (1994).
39. D.R. Entem, R. Machleidt, Phys. Rev. C **66**, 014002 (2002); Phys. Rev. C **68**, 041001 (2003).
40. E. Epelbaum, W. Glöckle, U.-G. Meissner, Nucl. Phys. A **747**, 362 (2005).
41. S.K. Bogner, T.T.S. Kuo, A. Schwenk, Phys. Rep. **386**, 1 (2003).
42. S.K. Bogner, A. Schwenk, R.J. Furnstahl, A. Nogga, Nucl. Phys. A **763**, 59 (2005).
43. G.A. Lalazissis, J. König, P. Ring, Phys. Rev. C **55**, 540 (1997).
44. V. Baran, M. Colonna, V. Greco, M. Di Toro, Phys. Rep. **410**, 335 (2005).
45. C. Mahaux, P.F. Bortignon, R.A. Broglia, C.H. Dasso, Phys. Rep. **120**, 1 (1985).
46. D. Lunney, J.M. Pearson, C. Thibault, Rev. Mod. Phys. **75**, 1021 (2003).
47. T. Frick, Kh. Gad, H. Müther, P. Czerski, Phys. Rev. C **65**, 034321 (2002).
48. E. van Dalen, C. Fuchs, A. Faessler, Phys. Rev. Lett. **95**, 022302 (2005).
49. J.M. Pearson, S. Goriely, Phys. Rev. C **64**, 027301 (2001).
50. D. Alonso, F. Sammarruca, Phys. Rev. C **67**, 054301 (2003); F. Sammarruca, W. Barredo, P. Krastev, Phys. Rev. C **71**, 064306 (2005).
51. C.J. Horowitz, B.D. Serot, Nucl. Phys. A **464**, 613 (1987).
52. H. Krivine, J. Treiner, O. Boghias, Nucl. Phys. A **336**, 155 (1980).
53. S. Goriely, E. Khan, Nucl. Phys. A **706**, 217 (2002).
54. S. Hama *et al.*, Phys. Rev. C **41**, 2737 (1990); E.D. Cooper *et al.*, Phys. Rev. C **47**, 297 (1993).
55. P. Danielewicz, Nucl. Phys. A **673**, 275 (2000).
56. T. Gaitanos, C. Fuchs, H. H. Wolter, A. Faessler, Eur. Phys. J. A **12**, 421 (2001).
57. P.K. Sahu, W. Cassing, U. Mosel, A. Ohnishi, Nucl. Phys. A **672**, 376 (2000).
58. H.F. Arellano, H.V. von Geramb, Phys. Rev. C **66**, 024602 (2002).
59. S. Typel, Phys. Rev. C **71**, 064301 (2005).
60. W. Zuo, L.G. Cao, B.A. Li, U. Lombardo, C.W. Shen, Phys. Rev. C **72**, 014005 (2005).
61. T. Gaitanos, M. Di Toro, S. Typel, V. Baran, C. Fuchs, V. Greco, H.H. Wolter Nucl. Phys. A **732**, 24 (2004).

62. L.-W. Chen, C.M. Ko, B.-A. Li, Phys. Rev. C **72**, 064606 (2005).

63. J.A. McNeil, J.R. Shepard, S.J. Wallace, Phys. Rev. C **27**, 2123 (1983).

64. A.M. Lane, Nucl. Phys. **35**, 676 (1962).

65. R. Kozack, D.G. Madland, Phys. Rev. C **39**, 1461 (1989); Nucl. Phys. A **509**, 664 (1990).

66. F. Rami *et al.* [FOPI Coll.], Phys. Rev. Lett. **84**, 1120 (2000).

67. W. Reisdorf *et al.* [FOPI Coll.], Phys. Rev. Lett. **92**, 232301 (2004).

68. W. Botermans, R. Malfliet, Phys. Rep. **198**, 115 (1990).

69. G.F. Bertsch, S. Das Gupta, Phys. Rep. **160**, 190 (1988).

70. C. Gregoire, B. Remaud, F. Sebille, L. Vincet, Y. Raffay, Nucl. Phys. A **465**, 317 (1987).

71. B. Blättel, V. Koch, U. Mosel, Rep. Prog. Phys. **56**, 1 (1993).

72. C. Fuchs, H.H. Wolter, Nucl. Phys. A **589**, 732 (1995).

73. J. Aichelin, Phys. Rep. **202**, 233 (1991); C. Hartnack *et al.*, Eur. Phys. J. A **1**, 151 (1998).

74. S.A. Bass *et al.*, Prog. Part. Nucl. Phys. **41**, 225 (1998).

75. J. Jaenicke, J. Aichelin, N. Ohtsuka, R. Linden, A. Faessler, Nucl. Phys. A **536**, 201 (1992).

76. H. Sorge, H. Stöcker, W. Greiner, Ann. Phys. **192**, 266 (1989).

77. A. Ono, H. Horiuchi, T. Maruyama, A. Ohnishi, Prog. Theor. Phys. **87**, 1185 (1992).

78. H. Feldmeier, J. Schnack, Rev. Mod. Phys. **72**, 655 (2000).

79. P. Danielewicz, Ann. Phys. **152**, 239 (1984); Ann. Phys. **152**, 305 (1984).

80. H.S. Köhler, Phys. Rev. C **51**, 3232 (1995).

81. K. Morawetz, P. Lipavský, V. Špička, Ann. Phys. **294**, 134 (2001).

82. K. Morawetz *et al.*, Phys. Rev. C **63**, 034619 (2001).

83. K. Morawetz *et al.*, Phys. Rev. Lett. **82**, 3767 (1999).

84. W. Cassing, S. Juchem, Nucl. Phys. A **665**, 377 (2000); Nucl. Phys. A **677**, 445 (2000).

85. J. Lehr, M. Effenberger, H. Lenske, S. Leupold, U. Mosel, Phys. Lett. B **483**, 324 (2000).

86. C. Fuchs, A. Faessler, M. El-Shabshiry, Phys. Rev. C **64**, 024003 (2001).

87. K. Morawetz, P. Lipavský, V. Špička, H.N. Kwong, Phys. Rev. C **59**, 3052 (1999).

88. Not present in bibliography

89. M. Debowski *et al.*, Z. Phys. A **356**, 313 (1996).

90. N. Herrmann, J.P. Wessels, T. Wienold, Ann. Phys. **49**, 581 (1999).

91. P. Danielewicz *et al.*, Phys. Rev. Lett. **81**, 2438 (1998); C. Pinkenburg *et al.*, Phys. Rev. Lett. **83**, 1295 (1999).

92. A. Andronic *et al.* [FOPI Coll.], Phys. Lett. B **612**, 173 (2005).

93. C. Fuchs, T. Gaitanos, Nucl. Phys. A **714**, 643 (2003).

94. P. Danielewicz, R. Lacey, W.G. Lynch, Science **298**, 1592 (2002).

95. A. Hombach, W. Cassing, S. Teis, U. Mosel, Eur. Phys. J. A **5**, 157 (1999).

96. A. Andronic *et al.* [FOPI Coll.], Nucl. Phys. A **661**, 333c (1999); Phys. Rev. C **64**, 041604 (2001); Phys. Rev. C **67**, 034907 (2003).

97. G. Stoica *et al.* [FOPI Coll.], Phys. Rev. Lett. **92**, 072303 (2004).

98. D. Brill *et al.* [KaoS Coll.], Zeit. f. Phys. A **355**, 61 (1996).

99. T. Gaitanos, C. Fuchs, H.H. Wolter, Nucl. Phys. A **741**, 287 (2004); Nucl. Phys. A **650**, 97 (1999); C. Fuchs, T. Gaitanos, H.H. Wolter, Phys. Lett. B **381**, 23 (1996).

100. G.Q. Li, R. Machleidt, Phys. Rev. C **48**, 1702 (1993); Phys. Rev. C **49**, 566 (1994).

101. A.B. Larionov, W. Cassing, S. Leupold, U. Mosel, Nucl. Phys. A **696**, 747 (2001).

102. B. Hong *et al.* [FOPI Coll.], Phys. Rev. C **71**, 034902 (2005).

103. T. Gaitanos, C. Fuchs, H.H. Wolter, Phys. Lett. B **609**, 241 (2005).

104. P. Danielewicz, Acta Phys. Polon. B **33**, 45 (2002).

105. B.-A. Li, Nucl. Phys. A **708**, 365 (2002); Phys. Rev. C **69**, 064602 (2004).

106. B.-A. Li, C.B. Das, S. Das Gupta, Ch. Gale, Phys. Rev. C **69**, 011603 (2004).

107. J. Rizzo, M. Colonna, M. Di Toro, Nucl. Phys. A **732**, 202 (2004).

108. L.-W. Chen, C.M. Ko, B.-A. Li, Phys. Rev. Lett. **94**, 032701 (2005).

109. D.V. Shetty, S.J. Yennello, G.A. Souliotis, [nucl-ex/0505011]

110. D.T. Khoa, H.S. Than, [nucl-th/0502059]; D.T. Khoa, W. von Oertzen, H.G. Bohlen, H.S. Than, [nucl-th/0510048].

111. B.-A. Li, G.-C. Yong, W. Zuo, Phys. Rev. C **71**, 044604 (2005).

112. B. Liu, V. Greco, V. Baran, M. Colonna, M. Di Toro, Phys. Rev. C **65**, 045201 (2002).

113. R. Stock, Phys. Rep. **135**, 259 (1986).

114. P. Senger, H. Ströbele, J. Phys. G **25**, R59 (1999).

115. V.S. Uma Maheswari, C. Fuchs, A. Faessler, L. Sehn, D. Kosov, Z. Wang, Nucl. Phys. A **628**, 669 (1998).

116. B.-A. Li, G.-C. Yong, W. Zuo, Phys. Rev. C **71**, 014608 (2005).

117. Q. Li, Z. Li, S. Soff, M. Bleicher, H. Stöcker, Phys. Rev. C **72**, 034613 (2005).

118. A. Schmah *et al.* [KaoS Coll.], Phys. Rev. C **71**, 064907 (2005).

119. J. Aichelin, C.M. Ko, Phys. Rev. Lett. **55**, 2661 (1985).

120. S.W. Huang, A. Faessler, G.Q. Li, R.K. Puri, E. Lehmann, D.T. Khoa, M.A. Matin, Phys. Lett. B **298**, 41 (1993).

121. C. Hartnack, J. Jaenicke, L. Sehn, H. Stöcker, J. Aichelin, Nucl. Phys. A **580**, 643 (1994).

122. G.Q. Li, C.M. Ko, Phys. Lett. B **349**, 405 (1995).

123. C. Fuchs, Z. Wang, L. Sehn, A. Faessler, V.S. Uma Maheswari, D.S. Kosov, Phys. Rev. C **56**, R606 (1997).

124. T. Maruyama, W. Cassing, U. Mosel, S. Teis, K. Weber, Nucl. Phys. A **573**, 653 (1994).

125. E. L. Bratkovskaya, W. Cassing, U. Mosel, Nucl. Phys. A **622**, 593 (1997).

126. J.T. Balewski *et al.* [COSY-11 Coll.], Phys. Lett. B **338**, 859 (1996); Phys. Lett. B **420**, 211 (1998).

127. D. Miskowiec *et al.* [KaoS Coll.], Phys. Rev. Lett. **72**, 3650 (1994).

128. C. Sturm *et al.* [KaoS Coll.], Phys. Rev. Lett. **86**, 39 (2001).

129. C. Fuchs, Prog. Part. Nucl. Phys. **56**, 1 (2006).

130. C. Fuchs, A. Faessler, E. Zabrodin, Y.M. Zheng, Phys. Rev. Lett. **86**, 1974 (2001); C. Fuchs, A. Faessler, S. El-Basaouny, E. Zabrodin, J. Phys. G **28**, 1615 (2002).

131. Ch. Hartnack, J. Aichelin, J. Phys. G **28**, 1649 (2002).

132. Ch. Hartnack, H. Oeschler, J. Aichelin, *Phys. Rev. Lett.* **96**, 012302 (2006).
133. D.J. Nice, E.M. Splaver, I.H. Stairs, O. Löhmer, A. Jessner, M. Kramer, and J.M. Cordes, *Astrophys. J.* **634**, 1242 (2005).
134. T. Kähn et al., [nucl-th/0602038].
135. A.W. Steiner, M. Prakash, J.M. Lattimer, P.J. Ellis, *Phys. Rep.* **411**, 325 (2005).
136. B.-A. Li, A.W. Steiner, [nucl-th/0511064].
137. J.M. Lattimer, C.J. Pethick, M. Prakash, and P. Haensel, *Phys. Rev. Lett.* **66**, 2701 (1991).
138. D. Blaschke, H. Grigorian, and D. Voskresensky, *Astron. Astrophys.* **424**, 979 (2004).
139. E.E. Kolomeitsev, and D.N. Voskresensky, *Nucl.Phys. A* **759**, 373 (2005).
140. S. Popov, H. Grigorian, R. Turolla and D. Blaschke, *Astron. Astrophys.* **448**, 327 (2006).